Performance Analysis of Anisotropic Scattering Center Detection

Randolph L. Moses, Eniz Erten, and Lee C. Potter

Department of Electrical Engineering
The Ohio State University
2015 Neil Avenue
Columbus, OH 43210 USA

ABSTRACT

We consider the problem of detecting anisotropic scattering of targets from wideband SAR measurements. We first develop a scattering model for the response of an ideal dihedral when interrogated by a wideband radar. We formulate a stochastic detection problem based on this model and Gaussian clutter models. We investigate the performance of three detectors, the conventional imaging detector, a generalized likelihood ratio test (GLRT) detector based on the dihedral anisotropic scattering model, and a sum-of-squares detector motivated as a computationally attractive alternative to the GLRT test. We also investigate the performance degradation of the GLRT detector when using truncated angle response filters, and analyze detector sensitivity to changes in target length. Finally, we present initial results of angular matched filter detection applied to UWB radar measurements collected by the Army Research Laboaratory at Aberdeen Proving Grounds.

Keywords: target detection, anisotropic, optimal detector, GLRT, UWB radar

1. INTRODUCTION

Conventional SAR imaging assumes an isotropic response from scattering centers. However, man-made targets often exhibit distinctly anisotopric scattering. There has been recent interest in exploiting anisotropic scattering behavior of man-made objects to improve target detection performance.[1–3] These techniques use the property that angular scattering response is inversely proportional to the width of the scattering object.

Conventional SAR (or ISAR) imaging aims to coherently sum received signal energy at each "pixel" in the formed image. The coherent summation is usually unweighted (or perhaps weighted by a window to minimize sidelobe effects). An unweighted sum can be shown to have the interpretation of an optimal detector for a scattering center that has an isotropic (constant) response as a function of view angle, for a certain clutter model.

On the other hand, it is known that many scattering mechanisms on man-made targets exhibit anisotropic responses as a function of angle. An optimal target detector should take this anisotropic scattering into account. This has been noted by researchers, and improved target detection using this idea has been demonstrated.[1–3]

In this paper we consider SAR target detection from wideband radar measurements, from a signal detection standpoint. We first develop a scattering model for the response of an ideal dihedral when interrogated by a wideband radar (the studies in 1,2 apparently use a single-frequency scattering model). We formulate a stochastic detection problem based on this model and appropriate clutter models. We then quantify the performance achievable by exploiting anisotropic scattering behavior for detection. We analyze the performance of three detectors, the conventional imaging detector, a generalized likelihood ratio test (GLRT) detector based on the dihedral anisotropic scattering model, and a sum-of-squares detector motivated as a computationally attractive alternative to the GLRT test. We also consider some computationally efficient variants of the GLRT test obtained by using truncated angle response filters, and analyze their statistical performance and robustness to mismatch of assumed target length. Finally, we present initial results of angular matched filter techniques applied to ultra-wideband radar measurements collected by the Army Research Laboaratory at Aberdeen Proving Grounds.

email: (randy,ertene,potter)@er4.eng.ohio-state.edu. This work was performed through collaborative participation in the Advanced Sensors Consortium sponsored by the U.S. Army Research Laboratory under Cooperative Agreement DAAL01-96-2-0001..

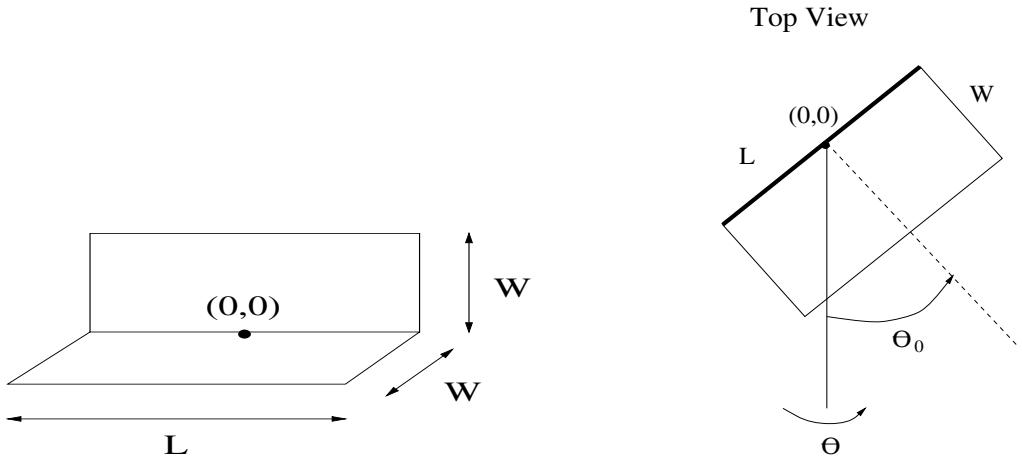

Figure 1. Geometry of the dihedral.

2. IDEAL RESPONSE FROM A DIHEDRAL

We first develop a model for anisotropic scattering that will form a basis for our detector design. We assume that the target scattering mechanism is a dihedral formed by two rectangular, perfectly conducting plates as shown in Figure 1. The vertex of the dihedral is of length L, and is oriented horizontally and at an angle θ_0 from the zero-angle reference $\theta = 0$. For convenience we assume that the zero phase reference point is the center of the vertex. We are interested in the monostatic scattering response for a radar oriented at an elevation angle of ϕ and angle θ with respect to broadside to the dihedral. The model is motivated because of the large dihedral-like response of ground targets at cardinal angles; it is hypothesized that this response is dominated by the dihedral formed by the ground and the vertical side of the target.

Because our radar is wideband, we are interested in the wideband response of the dihedral. To do so, we use physical optics (PO) to model the scattering $s(f, \theta)$ as a function of frequency and angle, and transform this data to obtain the response $s(t, \theta)$ in the time-angle domain. This model forms the basis of our detector design in the next section.

The return signal of such a dihedral of some length, say L, as a functon of aspect angle θ and frequncy f is given by the following equation

$$s(f, \theta) = A_o \, k \, \mathrm{sinc}(k \, L \, \sin(\theta - \theta_0)) \tag{1}$$

where $k = \frac{2\pi f}{c}$, A_o is a constant proportional to plate area and θ_0 is the orientation of the dihedral. We note that 1,2 employ the above model for a single frequency f_o. Assume that the radar transmits a waveform with frequency response $T(f)$ on $f \in [f_{min}, f_{max}]$ (The actual frequency response, $T(f)$, of the transmit signal used in UWB SAR is as shown in Figure 2). Then the backscattered waveform from the target, as a function of time t and radar orientation θ, is given by

$$s(t, \theta) = 2\mathrm{Re}(\tilde{s}(t, \theta)) \tag{2}$$

$$\tilde{s}(t, \theta) = \int_{f_{min}}^{f_{max}} T(f) s(f, \theta) e^{j2\pi f t} df \tag{3}$$

If we assume the transmitted signal is a constant over $[f_{min}, f_{max}]$, one can obtain a closed-form expression for the wideband dihedral scattering. By inserting 1 into 3 and carrying out the integration, we get :

$$\tilde{s}(t, \theta) = \frac{A_o F e^{j2\pi f_c t}}{L \sin(\theta - \theta_0) 2j} (e^{j2\pi f_c \frac{L}{c} \sin(\theta - \theta_0)} \mathrm{sinc}(\pi F (\frac{L}{c} \sin(\theta - \theta_0) + t)) - e^{-j2\pi f_c \frac{L}{c} \sin(\theta - \theta_0)} \mathrm{sinc}(\pi F (\frac{L}{c} \sin(\theta - \theta_0) - t))) \tag{4}$$

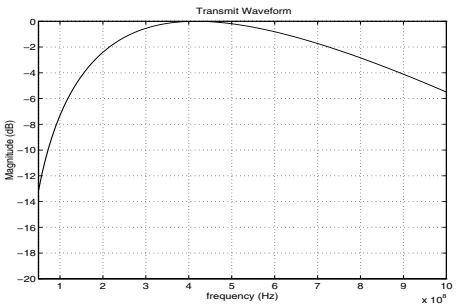

Figure 2. Transmit waveform, $T(f)$

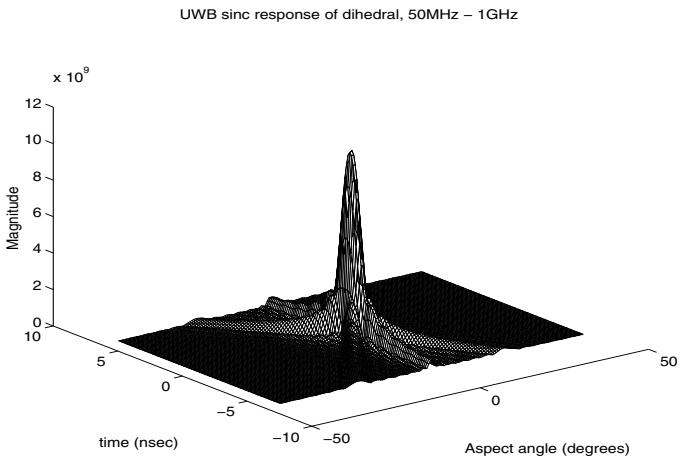

Figure 3. $\tilde{s}(t,\theta)$

where $F = f_{max} - f_{min}$ and $fc = \frac{f_{max}+f_{min}}{2}$. A plot of $\tilde{s}(t,\theta)$ is shown in Figure 3. We see that most of the scattered energy occurs near $t = 0$ and $\theta = 0$. The large response for $\theta = 0$ and $t \neq 0$ are sidelobes resulting from the assumed rectangular frequency response $T(f)$. The two diagonal ridges in $\tilde{s}(t,\theta)$ correspond to leading and trailing edge diffraction from the dihedral. $\tilde{s}(t,\theta)$ evaluated at $t = 0$ is given as follows :

$$\tilde{s}(0,\theta) = \frac{A_o \pi}{c}(f_{max}^2 - f_{min}^2)\text{sinc}(\pi\frac{L}{c}\sin(\theta-\theta_0)(f_{max} - fmin))\text{sinc}(\pi\frac{L}{c}\sin(\theta-\theta_0)(f_{max} + fmin)) \quad (5)$$

A plot of $\tilde{s}(0,\theta)$ given in Figure 4.

3. TARGET DETECTION AS A HYPOTHESIS TEST

Assume we have radar measurements from a wideband, angle-diverse radar. For each $k = 1,\ldots,N$, $y(t,\theta_k)$ is the time response (the received signal) at aperture location k; the time response might be measured directly (for an impulse radar) or obtained as the inverse Fourier transform from a linear FM chirp signal or a stepped frequency radar. The measured signal contains clutter $n(t,\theta_k)$, and may or may not contain a signal component $s(t,\theta_k)$ with unknown amplitude A. We consider the signal model in the previous section for general L, and as a special case the isotropic scattering response obtained with $L = 0$.

We model the clutter as white Gaussian noise with zero mean and variance σ^2 in the (t,θ) plane.As we show below, under this white noise assumption, one can obtain "matched filter" detectors that are optimal or close to optimal in the sense that they maximize the target detection probability for a given probability of false alarm. The

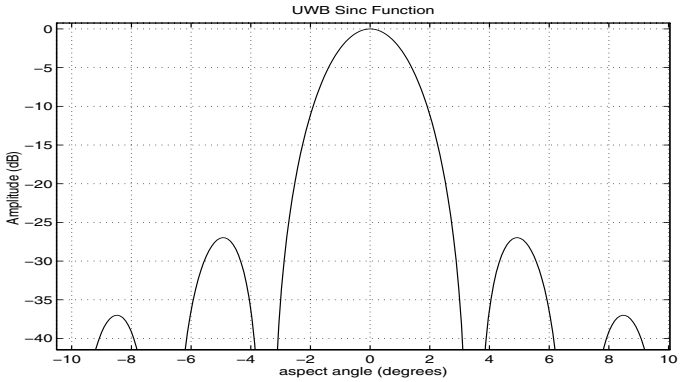

Figure 4. $|\tilde{s}(t,\theta)|$ for $t = 0$

Gaussian assumption is also motivated in part because $n(t,\theta_k)$ is the sum of a large number of clutter elements in the scene that lie on the surface of a sphere (whose radius corresponds to the two-way propagation time of the wavefront); because these clutter terms can reasonably be assumed to be independent, the clutter in this domain is approximately Gaussian by the law of large numbers. The white Gaussian assumption would not apply, however, if the clutter return is dominated by a small number of large-amplitude scattering mechanisms, and in fact the clutter is highly correlated in the (t,θ) plane in this case. A detailed study on the validity of a Gaussian white noise assumption, or the development of alternate clutter models, has not been carried out, although preliminary results by the authors and others suggests the white noise assumption is a reasonable starting point.[1–3]

We approach the target detection problem in the following way. The radar return signal corresponding to an image pixel traces out a hyperbola in the (t,θ) plane. Thus, the signal response from the time delay corresponding to a pixel is the signal $y(t,\theta_k)$ extracted along this hyperbolic path. Let $t(x,y,\theta)$ denote this hyperbola corresponding to pixel at location (x,y), and let

$$y_k = y(t(x,y,\theta_k),\theta_k), \qquad k = 1,\ldots N \tag{6}$$

$$y = [y_1,\ldots,y_N]^T \tag{7}$$

The task of target detection can be modeled as the following hypothesis test

$$\begin{aligned} H_0 &: \quad y = n \quad \text{(no target present)} \\ H_1 &: \quad y = As + n \quad \text{(target present)} \end{aligned} \tag{8}$$

where the vectors s and n are defined along the hyperbolic path similarly to y and A is an unknown target amplitude.

For target detection, we compute a detection statistic at each location (x,y). This set detection statistics can be displayed as an "image". For each location (x,y), the test statistic is formed as a function of the vector y defined in equation 7. SAR imaging can be interpreted as the computation of a decision statistic, at each pixel location, for solving the hypothesis problem given in equation 8. The inputs for imaging are the UWB time profiles $y(t,\theta_k)$ measured at each aperture position. The output is the array of decision statistics, which can be displayed as an image.

Below we consider three test statistics obtained from y and three corresponding detectors. The first is conventional imaging, and we determine the detection problem that conventional imaging is optimal for. We then consider a GLRT detector based on the dihedral response derived in the previous section. Finally, we consider a sum-of-squares detector motivated as a computationally simple alternative to the GLRT.

3.1. Conventional Imaging

In conventional imaging, the pixel value at location (x, y) is the coherent integration of SAR measurements along the hyperbolic path $t(x, y, \theta)$. This image value is thus given by (to within a constant):

$$d_1 = d_1(x, y) = \sum_{k=1}^{N} y(k)$$

This process can be thought of as filtering the signal with a uniform amplitude filter. If the signal component of y is $As = A[s(1) \dots s(N)]^T$, then the test statistic d_1 has probability distribution functions (pdfs) given by:

$$H_0 \quad : \quad d_1 \sim \mathcal{N}(0, N\sigma^2) \tag{9}$$

$$H_1 \quad : \quad d_1 \sim \mathcal{N}(A \sum_{i=1}^{N} s(i), N\sigma^2) \tag{10}$$

If the signal is an isotropic scatterer with amplitude A (*i.e.*, $s = A[1, \dots, 1]^T$), and if the clutter is white Gaussian noise in the (t, θ) plane, this filter is optimum (matched)[1–3] and the optimum detector is

$$d_1 \underset{\mathrm{H_0}}{\overset{\mathrm{H_1}}{\gtrless}} \eta$$

for some threshold η that is determined by the desired probability of false alarm; alternatively, a CFAR detection statistic can be used if σ^2 is unknown. The detection ROC curves corresponding to this detector can readily be found by varying η and computing the detection and false alarm probabilities from the distributions in equations 9 and 10. In fact, the above detector is uniformly most powerful for unknown A[4]; *i.e.* it is the detector that maximizes the probability of detection for a given probability of false alarm, independently of the value of A.

3.2. GLRT Detector

For a dihedral with known length L and orientation θ_0, the optimum detector is given by

$$d_2 \underset{\mathrm{H_0}}{\overset{\mathrm{H_1}}{\gtrless}} \eta$$

where

$$d_2 = \bar{s}^T(\theta_0) y$$

and $\bar{s}(\theta_0)$ is the vector formed from the dihedral response $s(t, \theta_k)$ sampled along the hyperbolic path corresponding to location (x, y), and scaled so that $\|\bar{s}^T(\theta_0)\| = 1$. In this case the test statistic is distributed as

$$H_0 \quad : \quad d_2 \sim \mathcal{N}(0, \sigma^2 \bar{s}^T \bar{s}) \tag{11}$$

$$H_1 \quad : \quad d_2 \sim \mathcal{N}(A \bar{s}^T s, \sigma^2 \bar{s}^T \bar{s}) \tag{12}$$

Again, this detector is uniformly most powerful for unknown amplitude A.

In practice, the orientation angle θ_0 is unknown. It would be nice to find a detector that is uniformly most powerful for unknown A and θ_0, but unfortunately no such detector exists. Therefore, we propose the popular (but suboptimal) generalized likelihood ratio test (GLRT) statistic

$$\hat{d}_2 = \bar{s}^T(\hat{\theta}_0) y \tag{13}$$

where $\hat{\theta}_0$ is the maximum likelihood (ML) estimate of θ_0, given by

$$\hat{\theta}_0 = \arg\max_{\phi} \bar{s}(\theta)^T y \tag{14}$$

Thus, the GLRT detector is given by

$$\max_{\theta} \bar{s}(\theta)^T y \underset{\mathrm{H_0}}{\overset{\mathrm{H_1}}{\gtrless}} \eta \tag{15}$$

Closed-form expressions for the distribution of $\hat{d}_2$ under H_0 and H_1 are not known; however, performance for the GLRT is bounded by the analytical performance bounds given above for the known θ_0 case.

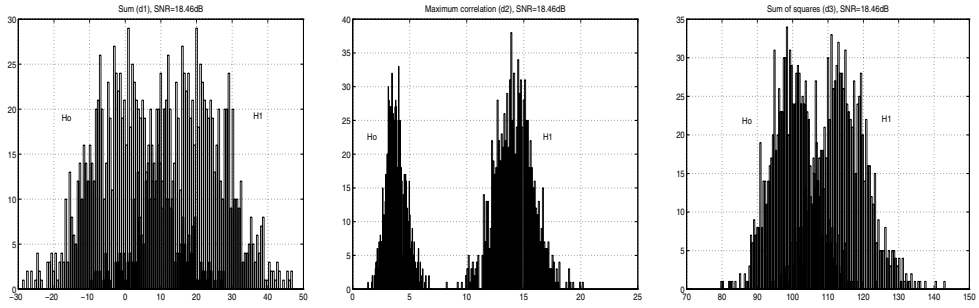

(a) Conventional Image (b) GLRT : d_2 (c) Sum-of-Squares : d_3

Figure 5. Detection statistic histograms for the three detection statistics

3.3. Sum of Squares Imaging

A computationally simple but suboptimal detector motivated by the GLRT detector is to compute each detection statistic as a sum of squares of the data vector:

$$d_3 = \frac{1}{\sigma^2}\sum_{k=1}^{N} y^2(k) = \frac{1}{\sigma^2} y^T y$$

The statistic d_3 is found to be central- and noncentral-χ^2 distributed under H_0 and H_1 [4]:

$$H_0 \quad : \quad d_3 \sim \chi^2_N \tag{16}$$

$$H_1 \quad : \quad d_3 \sim \chi^2_N(d^2) \tag{17}$$

The advantage of this detector is that there is minimal impact to conventional SAR image formation; one simply takes the square of the data $y(t, \theta_k)$ before summation. Thus, fast algorithms for image formation (*e.g.,*[5]) can also be used for fast computation of this test statistic.

It can be seen that for high signal-to-clutter ratio, $y \simeq s$ (to within a constant), the detection performance of the sum-of-squares (SoS) and GLRT detectors will be similar. On the other hand, the SoS detector statistic is not a function of target orientation θ_0, so we need only compute the statistic once, and not for several candidate θ_0 values as in the GLRT.

3.4. Performance Comparison

We present an example to illustrate the detection peformance gain in using the GLRT and sum-of-squares detectors over conventional imaging. We consider a dihedral with length $L = 5\,m$ and signal-to-clutter (SCR) ratio of 18.46dB (SCR is defined as $\sqrt{\frac{\sum_i s_i^2}{\sigma^2}}$). Figure 5 shows histograms of target and clutter for test statistics d_1, $\hat{d}_2$, d_3. We see improved target and clutter separability using the GLRT. The SoS detector performance is between the conventional imaging and GLRT performance, but is computationally nearly equivalent to the (simpler) imaging detector. For higher SCR, the SoS performance is closer to the GLRT performance.

We should note that none of the above detectors is optimal because they all use only a single hyperbolic slice of the given data $y(t, \theta_k)$. Since the target scattering response is nonzero for points off of this hyperbola (see Figure 3), some performance gain can be realized by using a detector on the full two-dimensional imagery. On the other hand, most of the target energy is concentrated in the considered hyperbolic slice, as can be seen from Figure 3, so the resulting performance loss is minimal (and the computational gain realized by restricting to a single hyperbolic slice is significant).

Table 1 summarizes the distributions of the three test statistics considered in this section.

Imaging technique	output for no target	output for target
Conventional Imaging	$d_1 \sim \mathcal{N}(0, N\sigma^2)$	$d_1 \sim \mathcal{N}(A\sum_{i=1}^{N} s(i), N\sigma^2)$
GLRT Imaging (for $\theta = \theta_0$)	$d_2 \sim \mathcal{N}(0, \sigma^2 \bar{s}^T \bar{s})$	$d_2 \sim \mathcal{N}(A\bar{s}^T s, \sigma^2 \bar{s}^T \bar{s})$
Sum-of-Squares Imaging	$d_3 \sim \chi^2_N$	$d_3 \sim \chi^2_N(d^2)$

Table 1. PDF's of the decision statistics for the three imaging procedures

4. GLRT PERORMANCE

In this section we consider the GLRT detector and some computationally efficient approximations obtained by truncating the detector "filter". We consider the performance degradation caused by the filter truncation, and also consider the performance sensitivity to mismatch between the assumed and actual target length L.

A filter whose impulse response is as given in equation 5 has to be employed (matched filter). Since the orientation angle θ_0 of the target is unknown, the GLRT detector is implemented as a bank of filters, each corresponding to a different orientation angle. The pixel value is taken to be the maximum of the outputs of this bank of filters. The filter with the maximum ouput gives the maximum likelihood estimate of the target orientation.[6]

As a computational saving, the matched filter may be truncated at, say, its 3dB points.[1,3] Let $h1$ denote the matched filter and $h2$ the 3dB truncated matched filter. As a further computational saving, $h2$ can be approximated by a uniform amplitude filter, denoted by $h3$ (see Fig.6). In either case, the filter bank above is replaced by a convolution operation: the vector $y = \{y(i)\}_{i=1}^{N}$, treated as a one-dimensional signal, is convolved with the filter h_2 or h_3, and the detector statistic is the maximum of the convolution output.

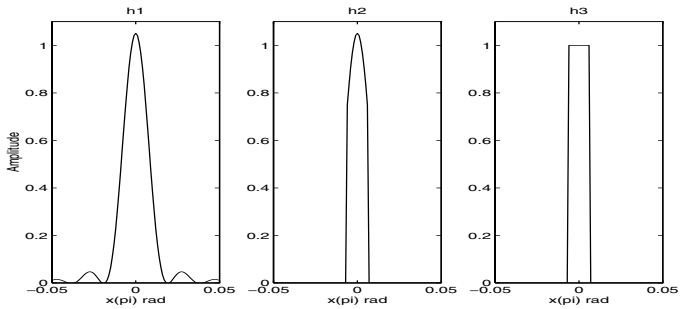

Figure 6. Filters $h1$, $h2$ and $h3$.

The optimal filters used to detect the target will be arbitrary to within a scaling constant. However, for optimum detection, the parameter L used to design the filter and actual length of the target have to be the same. In the case of a length mismatch, a loss in detection performance will be incurred. This loss can be conveniently observed in the ROC curves and the filter output SCR ratio. If the truncated filters are used, there will also be a loss in output SCR ratio, and a corresponding loss in performance. The expression for the probability of detection (P_D) for given probability of false alarm is directly proportional to the SCR, therefore the highest SNR will coincide with the highest P_D.

To quantify this loss, Figure 7(a) shows the ouput SNR as a function of filter L for all three filters. The filters are designed assuming $L_D = 5m$, and tested with a measured signal that corresponds to a dihedral with varying L. The baseline (0 dB level) is chosen as the matched filter output SCR corresponding to each input signal. The clutter is modeled as additive white Gaussian. For a perfect signal-filter match,the loss incured by using $h2$ and $h3$ versus the matched filter is about -1dB. However, when the target length is about 50% larger than the filter L, $h2$ and $h3$ outperform $h1$. Thus, for best performance, the filters $h2$ and $h3$ should be designed for about 50% larger length than the expected target length. The performance of the three filters when $h2$ and $h3$ are designed to have best

performance at $L = 5m$ is shown in Figure 7(b). The best performance obtained by $h2$ is about 0.25 dB less than the optimum performance and the best performance obtained by $h3$ is 0.5 dB less than the optimum performance. Furthermore, these filters are relatively insensitive to variations in target length; the ouput SCR decreases only $1dB$ when the length of the target increases or decreases by a factor of 2.

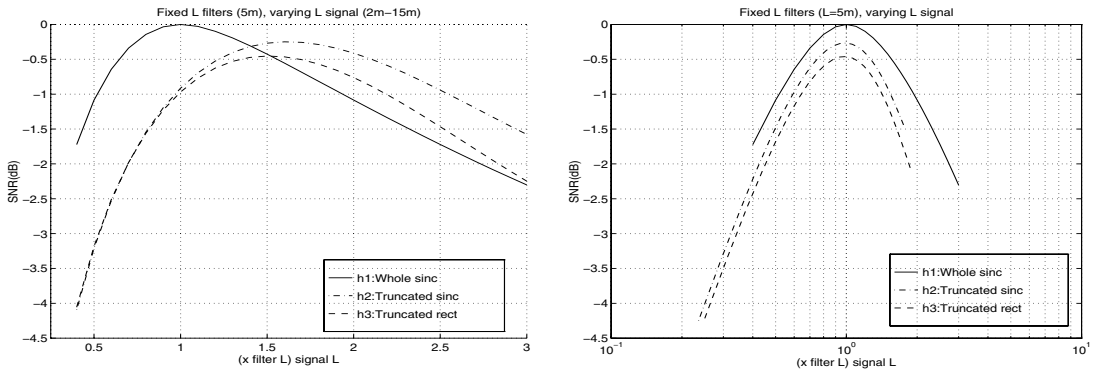

(a) (b)

Figure 7. Output SCR as a function of L/L_D; (a) filters designed assuming $L_D = 5$ meters, (b) as in (a) but with $h2$ and $h3$ filters compensated to give peak performance at $L_D = 5$ meters.

Another way to measure the loss caused by target length mismatch or truncation of the matched filter is to compare the corresponding detection ROC curves. Figure 8 shows these ROC curves for the case considered in Figure 7. Figure 8(b) shows the ROC curves when the target and filter design values of L coincide, for the three filters $h1$, $h2$ and $h3$ (for $h2$ and $h3$ we compensate the design L value to obtain best performance, as in Figure 7(b)). Figure 8(a) shows ROC curves for $h1$ when designed for a dihedral of $L = 5$ meters, when the measured dihedral has lengths of L=3, 5 and 10 meters.

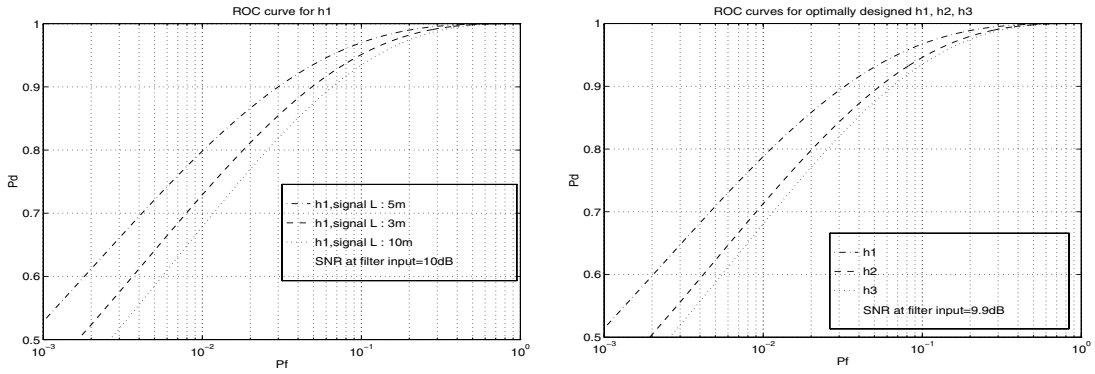

(a) (b)

Figure 8. Detection ROC curves for (a) matched filter but with target length mismatch, and (b) matched filters $h1$, and truncated filters $h2$, and $h3$ when measured target length matches filter design length.

5. MEASURED DATA

In this section we present preliminary results obtained by applying the anisotropic scattering detectors to measured UWB imagery. The SAR measurements were collected by Army Research Laboratory at Aberdeen Proving Grounds.

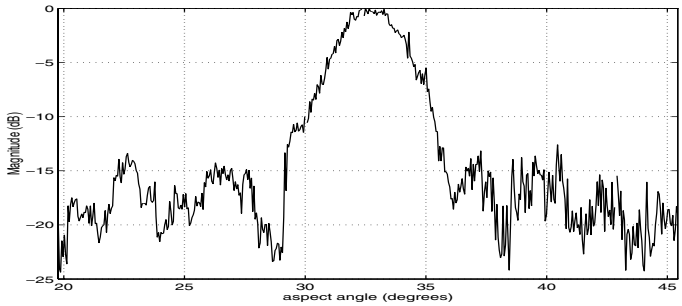

Figure 9. Flash response from a dihedral

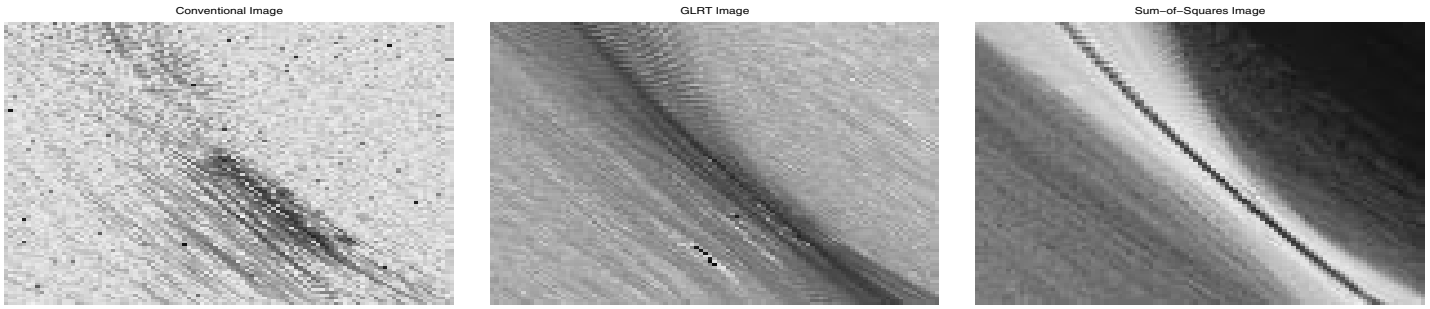

(a) Conventional Image (b) GLRT Image (c) Sum-of-Squares Image

Figure 10. UWB imagery

The images shown are of a target oriented approximately -32° from the SAR aperture.

Figure 9 shows the anisotropic scattering return signal from the target along the hyperbolic path corresponding to the location of the center of the "dihedral". This response shows good agreement with the wideband model in Section 2 in the mainlobe region. The model sidelobes are lower than the measured sidelobes; the reason for this is not yet clear and is under investigation. However, this difference will have a minor impact on detection performance because it is in a low-energy region. Figure 10 shows "images" of detection statistics d_1, d_2, and $d_{3'}$ in a region around the target. Finally, Figure 11 shows histograms for these detection statistics in the target and background regions. While this imagery is clearly anecdotal (presenting results for only one target realization), it does suggest that improved target detection may be realized using the SoS and GLRT detectors.

6. CONCLUSIONS

We have considered SAR precreeening by detecting anisotropic scattering. We have viewed the problem as an optimal or suboptimal binary hypothesis testing problem. We developed a wideband scattering model for dihedrals, and obtained a closed-form expression, based on the dominant term of a physical optics scattering model for a dihedral. Using this model, along with a white Gaussian clutter model for clutter in the (t, θ) domain, we considered three detectors: conventional imaging, a GLRT detector "matched" to the target anisotropic scattering response at its center, and a sum-of-squares detector. We also considered computationally efficient approximations to the GLRT detector obtained by truncating the matched filter.

From analytical studies on an ideal dihedral scattering model, we quantified performance of the above three detectors. In particular, we quantified detection performance gain achievable using anisotropic scattering detectors, and quantified this gain as a function of target length. We also considered sensitivity and robustness of the GLRT detector by analyzing the performance loss due to truncating the GLRT detection filter, and due to changes in the

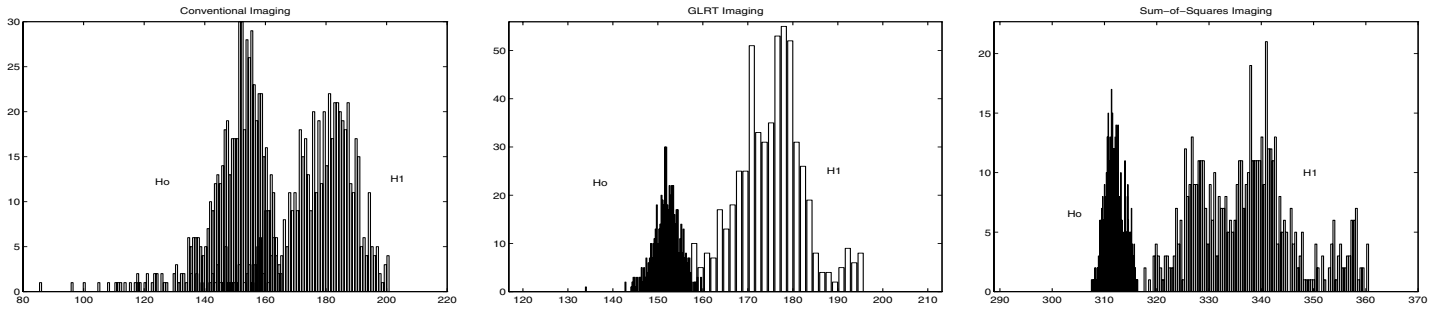

(a) Conventional Imaging (b) GLRT Imaging (b) Sum-of-Squares Imaging

Figure 11. Histograms of UWB imagery

target length. We showed that the performance loss was minimal — less than 0.5 dB for filter truncation, and approximately 1 dB for changes in target length up to a factor of two.

Finally, we presented preliminary studies of anisotropic detection on UWB radar measurements from ARLs impulse radar operating as a boom SAR at Aberdeen Proving Grounds. The results, shown for a ground target, are encouraging, and corroborate promise shown by the analytical studies for using anisotropic scattering detectors.

Our future work is focused on more extensive analysis of the ARL data, and comparing the quantitative analytical results with results obtained on measured data.

REFERENCES

1. M. R. Allen and L. E. Hoff, "Wide-angle wideband sar matched filter image formation for enhanced detection performace," in *Algorithms for Synthetic Aperture Radar Imagery*, vol. 2230, pp. 302–314, SPIE, (Orlando FL), Apr. 1994.
2. M. R. Allen, J. M. Jauregui, and L. E. Hoff, "FOPEN-SAR detection by direct use of simple scattering physics," in *Proceedings of the SPIE International Symposium on Algorithms for Synthetic Aperture Radar Imagery II*, D. A. Giglio, ed., vol. 2487, pp. 45–55, (Orlando, FL), Apr. 1995.
3. R. D. Chaney, A. S. Willsky, and L. M. Novak, "Coherent aspect-dependent sar image formation," in *Algorithms for Synthetic Aperture Radar Imagery*, vol. 2230, pp. 256–274, SPIE, (Orlando FL), Apr. 1994.
4. L. L. Scharf, *Statistical Signal Processing*, Addison-Wesley, 1991.
5. J. McCorkle and M. Rofheart, "An order $n^2 \log(n)$ backprojection algorithm for focusing wide-angle, wide-bandwidth, arbitrary motion synthetic aperture radar," in *Radar Sensor Technology*, vol. 2747-05, SPIE, 1996.
6. D. H. Johnson and D. E. Dudgeon, *Array Signal Processing : concepts and techniques*, Prentice Hall, Englewood Cliffs, NJ, 1993.